Ultrafast X-ray absorption study of longitudinal-transverse phonon coupling in electrolyte aqueous solution

Jiao, Yishuo; Adams, Bernhard W.; Dohn, Asmus Ougaard; Møller, Klaus Braagaard; Jonsson, Hannes; Rose-Petruck, Christoph

Published in:
Physical Chemistry Chemical Physics

Link to article, DOI:
10.1039/c7cp02978k

Publication date:
2017

Document Version
Peer reviewed version

PCCP

ARTICLE

Ultrafast X-ray Absorption Study of Longitudinal-Transverse Phonon Coupling in Electrolyte Aqueous Solution

Received 00th January 20xx,
Accepted 00th January 20xx

DOI: 10.1039/x0xx00000x

www.rsc.org/

Yishuo Jiao[a], Bernhard W. Adams[b]†, Asmus Ougaard Dohn[c], Klaus B. Møller[d], Hannes Jónsson[c], Christoph Rose-Petruck*[a]

Ultrafast x-ray absorption spectroscopy is applied to study the conversion of longitudinal to transverse phonons in aqueous solution. Permanganate solutes serve as X-ray probe molecules that permit the measurement of the conversion of 13.5-GHz, longitudinal phonons to 27-GHz, transverse phonons that propagate with high-frequency sound speed. The experimental results, combined with QM/MM MD simulations, show that the hydrogen bond network around the charged solutes has a glass-like stiffness that persists for at least tens of picoseconds.

Introduction

The hydrogen bonds (HBs) in aqueous solutions can locally adopt an ordered tetrahedral arrangement[1] and thereby have glass-like stiffness on a short timescale reflected in spectroscopic and mechanical properties.[2-4] The effect of solutes on the HB network of water still remains contentious. Omta and Bakker *et al.*[5] conducted vibrational mid-infrared spectroscopy to aqueous ion solutions and concluded that ions will only perturb the immediate vicinity of ions and the aqueous solutions can be treated as colloidal suspensions of "particles" composed of solute molecule and its first one or two hydration shells. This conclusion, however, is in contradiction with the conclusions of Chen *et al.* who conducted Femtosecond elastic second harmonic scattering (fs-ESHS) experiments to probe the long-range correlation effects of water dipole moments in aqueous solutions.[6] The scattering data, together with simulations, led them to the conclusion that the ions induce long-range perturbation effects in the hydrogen bond network up to more than 70 hydration layers of the solute molecules. Small Angle X-ray Scattering (SAXS) results also reveal the existence of inhomogeneities in aqueous solutions of polyatomic anions.[7] More details and relevant conclusions made in this field were previously reviewed by Y. Marcus. [8]

The coherent oscillations of atoms in liquids are often referred to as phonons, analogous to the solid state. For instance, Elton *et al.* conducted molecular dynamics simulations of liquid water and concluded that optical phonons can propagate along the hydrogen bond network. The coherent oscillations of water molecules can serve as an explanation of the peak assignment discrepancies between IR/dielectric and Raman water spectra.[2] D. Shelton proposed the longitudinal-orientational coupling of phonons in water for the explanation of the water dipole moment long-range correlation effects observed in HRS experiments.[9] Phonons were also used as a probe of the structural properties of water. For instance, it has long been found by both experimental and theoretical studies that sound waves of high enough frequency can propagate in liquid water with a so-called "fast-sound" speed, i.e. a speed twice as high as the normal sound speed.[4, 10-12] Viscoelastic theory has been used to explain this phenomenon. According to this theory, the HB network will respond to the high-frequency phonons with glass-like stiffness when the sound frequency is higher than a specific frequency.[11, 12] The reciprocal of this angular frequency is the structural relaxation time of the liquid. Thus, measurement of the sound propagation speed as a function of frequency yields an estimate of the structural relaxation time. The value for neat water at room temperature is about 0.6 ps and the structural relaxation is attributed to local rearrangements of the hydrogen bond network.[11, 12] In the experiments reported here, phonons of known wavenumber are generated in the electrolyte solutions with laser-pulse-induced Stimulated Brillouin Scattering (SBS), as will be discussed below. The phonons were used as a characterization of the properties of HB network around the solutes such as their structural relaxation time and stiffness.

Methods

Pump-probe experiments were conducted at 7ID-C of the Advanced Photon Source, Argonne National Laboratory. The pump pulses were generated with a laser consisting of a

[a] Department of Chemistry, Brown University, 324 Brook St., Box H, Providence, RI 02912, USA
[b] Argonne National Laboratory, 9700 S. Cass Ave, Argonne, IL 60439, USA
[c] Faculty of Physical Sciences, VR-III, University of Iceland, 107 Reykjavik, Iceland
[d] Department of Chemistry, Technical University of Denmark, Kemitorvet 207, DK-2800 Kgs. Lyngby, Denmark
† Current Address: Incom, Inc.294 Southbridge Rd, Charlton, MA 01507, USA

Ti:sapphire laser oscillator (Coherent Mira), and a Coherent Legend regenerative amplifier pumped by a Coherent Evolution laser. The oscillator was phase-locked to the APS master clock and had a frequency of 88 MHz. The amplified laser pulses were frequency-tripled from 800 nm to 266 nm and used for pumping the sample. The 50-fs laser pulses were focused into a 70-µm diameter spot with a peak intensity of 10^{13} W/cm². A monochromatic X-ray pulses emitted from the synchrotron were 100-150 ps long and were used as probe pulses transmitted through the liquid sample. In the sample chamber, the laser beam was overlapped co-linearly with the X-ray beam and intersected perpendicularly the liquid sample jet. The sample was at room temperature, about 300 K.

The transmitted X-ray beam was detected by a streak camera with about 2 ps temporal resolution. The streak camera consisted of a high-vacuum chamber with transmission-type CsI photocathode, a pair of meandering-stripline deflection plates, a magnetic lens for imaging the electrons from the entrance slit to the detector, a set of secondary deflection plates for dark-gating, etc., and an in-vacuum back-illuminated Princeton Instrument Pixis 400B CCD camera.[13] X-ray pulses striking the photocathode at normal incidence produced photoelectrons with electron densities proportional to the incident X-ray intensity. The electrons were then accelerated, transported through the deflection plate region, and focused by the magnetic lens onto the CCD camera. Pulses from the laser oscillator at 88 MHz repetition rate were used to trigger the streak camera, which was therefore not influenced by any laser amplifier jitter. A 100-ps photodiode was used to detect these laser pulses. A microwave amplifier chain was used to capture the signal from the photodiode and produce a fast voltage ramp for fast electron deflection. By deflecting the photoelectrons, the time information was converted into spatial information. The in-vacuum, back-illuminated CCD camera was directly exposed to the photoelectrons, ensuring minimum detection noise. 20 s exposure times were used to yield CCD readout images with up to 12k counts per pixel.

Each pump laser pulse was located temporarily in the middle of the X-ray pulse. Thus, each X-ray pulse streak measured the entire temporal evolution of the sample before and after laser pulse excitation. Besides the laser and X-ray, the streak camera was also synchronized with pump-probe pulses in time domain. Specifically, X-ray pulse transmitted through the excited sample was streaked. In between each laser pulse an X-ray pulse transmitted through the un-pumped sample was streaked. Helmholtz coils surrounding the streak camera were used to periodically shift the positions of the electron streaks on the CCD camera depending on whether the sample solution was laser-excited or not. The deflection induced by the Helmholtz coils lead to an offset to the streaks positions by a few millimeters on the CCD-detector. By doing that, each camera image contains two parallel streaks, one from the pumped and one from the un-pumped sample. These two streaks can then be analyzed by normalizing the pump-probe streaks with the non-pump-probed streaks. The normalized changes of X-ray transmittance $\Delta T(t)$ were then calculated with the streak intensity $I_{pumped}(t)$ of the pumped sample and the streak intensity $I_{ref}(t)$ of the un-pumped sample as in equation (1):

$$\Delta T(t) = \frac{I_{pumped}(t) - I_{ref}(t)}{I_{ref}(t)} \quad (1)$$

With the same experimental setup, a series of images were collected with the pump laser beam mechanically blocked from ever reaching the sample. These "flatfield" image data were acquired and processed identically to the pump-probe data. The "flatfield' data show a constant transmittance change $\Delta T_{flat} = 0 \pm 0.05\%$ (std. dev) for a data acquisition time of 50 minutes. More technical details are published in earlier publications.[13-15] Potassium permanganate (ACS reagent, ≥99.0%) was purchased from Sigma-Aldrich. Using distilled water provided by Argonne National Lab, 50 mM $KMnO_4$ aqueous solutions were prepared and used as liquid samples. Throughout the data acquisition process, the sample solution was circulated with a pump system. The solution flowed through a 450 µm quartz nozzle into the laser/X-ray interaction region inside a gas-sealed chamber flushed with nitrogen gas.

Theoretical studies were conducted using a combination of QM/MM Molecular Dynamics (QM/MM MD) and X-ray Absorption Spectra (XAS) simulations. Specifically, equilibrated solute-solvent structures were obtained from QM/MM molecular dynamics simulations (QM/MM MD). The permanganate ion was initially structurally relaxed with DFT in the Grid-based Projector Augmented Wave code (GPAW)[16, 17], with a real space grid spacing of 0.13 Å, and a complementary basis dzp-size basis of linear combinations of atomic orbitals as an initial guess of the pseudo wave functions.[16-18] The functional used was PBE[19], and a fermi-dirac distribution with a width of 0.05 eV on the occupation numbers, to ensure robust SCF convergence for the dynamics simulations. The relaxed ion structure was then placed in 10 cubic boxes of 25 Å side lengths containing 522 water molecules, pre-equilibrated to 300 K in the NVT ensemble using the TIP3P force field and Langevin type thermostat, implemented in the Atomic Simulation Environment (ASE)[20]. Water molecules within 3.5 Å of any of the ion atoms were removed. The 10 simulation boxes were then re-equilibrated using electrostatically embedded QM/MM MD.[21-23] The ion is modelled with the same parameters as in the structural relaxation, apart from the addition of non-bonded force field parameters needed for the additive QM/MM MD scheme, and a larger grid spacing of 0.18 Å, to increase the computational efficiency, and since so-called 'eggbox-effects' of the real space grid (small changes in energy and forces with respect to atomic positions relative to grid points) will average out in the thermal sampling. The parameters were taken from the UFF force field.[24]. Using Langevin dynamics and a timestep of 2 fs, the simulation boxes were re-equilibrated to 300 K within 2 ps, and production runs

could begin, with the same parameters. Altogether, the solvation shell was sampled for 68 ps. Ten equally spaced snapshots were then taken along the equilibrated molecular dynamics trajectories for further XAS calculation and analysis. Single molecular structure of MnO_4^- was also obtained with GPAW optimization for XAS calculation.

The theoretical calculations for the X-ray absorption spectra were done with FEFF9.6.[25-27] Full multiple scattering[28] was done with self-consistent field atomic potentials[27]. For both the FMS and SCF calculation processes, we set the sphere radius to be 6.0 Å around the Mn Center. The Hedin-Lundqvist electron self-energy was used for the energy dependent exchange correlation potentials in the XANES calculation. Finally, to account for the many-body interaction effects, the amplitude reduction factor (S_0^2) was set to 1 uniformly in all the calculations.

Results

The time-resolved dynamics of 50-mM $KMnO_4$ aqueous solution were measured at 300K. The solvated MnO_4^- anions served as probes for measuring the response of surrounding water molecules after impulsive excitation of phonons in the solution. The transmission changes of the solution were measured around the MnO_4^- 1s → 3d pre-edge absorption line (6542.8 eV). This formally forbidden dipole transition has non-vanishing oscillator strength because the tetrahedral symmetry of the complex permits mixing with p-orbitals.[29] Any distortion of the symmetry of the complex results in a change of the X-ray absorption cross section at this spectral position. We used the permanganate's X-ray absorption sensitivity to deformations as a surrogate marker for the motions of the complex. Since permanganate is hydrogen bonded to the surrounding water molecules, the complex's motions are strongly coupled to the surrounding water. Pre-edge absorption of X-rays promotes an inner-shell electron into the solute's LUMO, which overlaps with orbitals of the molecules in the solvation shell.[30] Therefore, the X-ray absorption cross section change of the permanganate pre-edge peak probes the dynamics of the surrounding water. It is noted that XAS, which we are applying here, is a linear spectroscopy, thus following the Beer–Lambert law: the transmittance change we observed is determined by the number density of our sample molecules along the probing path and the absorption cross sections of these molecules. During our tens of picoseconds observation time window, any change of the solute molecules' number density due to mass flow will be small and thus can be neglected. Consequently, any transmittance change observed here should be a reflection of the structural change of the sample molecules and the solvent shells as discussed above. By carrying out XAS measurements in the time domain, signals that decay quickly can be more easily detected than with frequency-domain measurements where they would be broadened and hard to find. More importantly, by placing probe ions in the solution and using XAS, phonons propagating locally can be observed. As a result, small wave-vector phonons were successfully detected with energies of 351 μeV and wave-vectors as low as ~0.062 nm^{-1}, corresponding to a 100-nm acoustic wavelength at the liquid water sound speed of on about 1.35 km/s.

The phonons are created by impulsive stimulated Brillouin scattering[31] of 266-nm, 50-fs laser pulses. The intensity of the laser light on the sample was about 10^{13} W/cm², which lead to substantial electrostriction.[32] Stimulated Brillouin scattering (SBS) is most intense in the backward and forward directions.[33] Within the pulse length of the laser beam the backward scattered light will interfere with the incoming light, creating an interference grating in the backward scattering direction

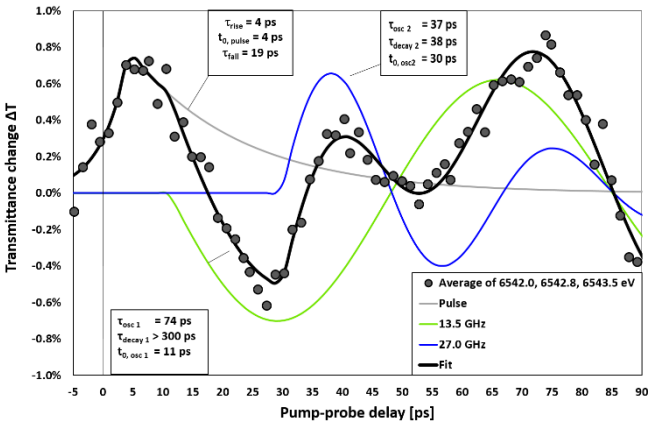

Figure 1 Changes of the X-ray transmittance at the manganese pre-edge absorption line vs. time after laser excitation. A fit to the data points is shown in black. The green line represents an oscillatory signal with 13.5-GHz and is interpreted as the fundamental oscillation. The blue line represents the 27-GHz oscillation and is identified as Second Harmonic (SH) phonon generation.

with a period $\lambda_{grating} = \lambda_{laser}/2n$, with n as the index of refraction of the solution. As a consequence, phonons are emitted predominantly with an acoustic wavelength $\lambda_{acoustic} = \lambda_{grating}$. The phonons are not necessarily spatially coherent because they are generated at random positions in the sample. Thus, phonons are not necessarily going to add up to a spatially coherent acoustic wave, which is what happened in the more common SBS driven by two interfering laser beams. Yet, it is important that the phonons are coherent in time because they are produced almost simultaneously with a short femtosecond pulse. Since we are probing the phonons with a local solute probe, the possible lack of spatial coherence is not a problem because measured oscillations are in phase with respect to the detection time.

FIG. 1 shows the measured transmittance change $\Delta T(t)$ with data points every 1.3 ps. The data points are the average of transmittances measured the pre-edge peak maximum (6542.8 eV) as well as 0.7 eV above and 0.8 eV below this peak. $\Delta T(t)$ is fitted as the sum of three functions, shown in equation (1): one double-exponential (pulse) function and two dampened sinusoidal functions. The sum of the fitted functions was plotted as a black line.

$$\Delta T(t) = T_{pulse} \cdot P(t) + T_{osc\,1} \cdot Osc_1(t) + T_{osc\,2} \cdot Osc_2(t) \quad (2)$$

$$with \quad P(t) = \begin{cases} e^{\left(\frac{t-t_{0,pulse}}{\tau_{rise}}\right)} & for \;\; t \le t_{0,pulse} \\ e^{-\left(\frac{t-t_{0,pulse}}{\tau_{fall}}\right)} & for \;\; t > t_{0,pulse} \end{cases}$$

$$and \;\; for \; i = 1,2 \quad Osc_i(t) = \begin{cases} 0 & for \;\; t \le t_{0,osc\,i} \\ e^{-\left(\frac{t_{0,osc\,i}-t}{\tau_{decay\,i}}\right)} sin\left(2\pi \frac{t-t_{0,osc\,i}}{\tau_{osc\,i}}\right) & for \;\; t > t_{0,osc\,i} \end{cases}$$

At zero delay-time, the transmittance changes with a nearly instrument-limited exponential rise with a time constant τ_{rise} of 4 ps followed by an exponential decay with a time constant τ_{rise} of 19 ps. A 13.5-GHz wave is produced 11ps after excitation. A quarter period later, at 30 ps, a wave with twice the frequency is measured. The oscillations with tens of gigahertz frequency is too slow to correspond to any single molecular movement and can only be from a coherent oscillation from a group of atoms/molecules. We identified these waves as the fundamental and second harmonic (SH) acoustic phonons. The initial pulse is caused by the intense laser radiation, which induces strong electrostriction, sample heating and solute-specific reactions such as charge transfers to solvent and ligand dissociations. The decay time constant is consistent with thermal relaxation but details cannot be extracted from these data, nor are these events the focus of this study. Instead, we focus on the evolution of phonons after the laser excitation.

As was discussed above, phonons are produced by

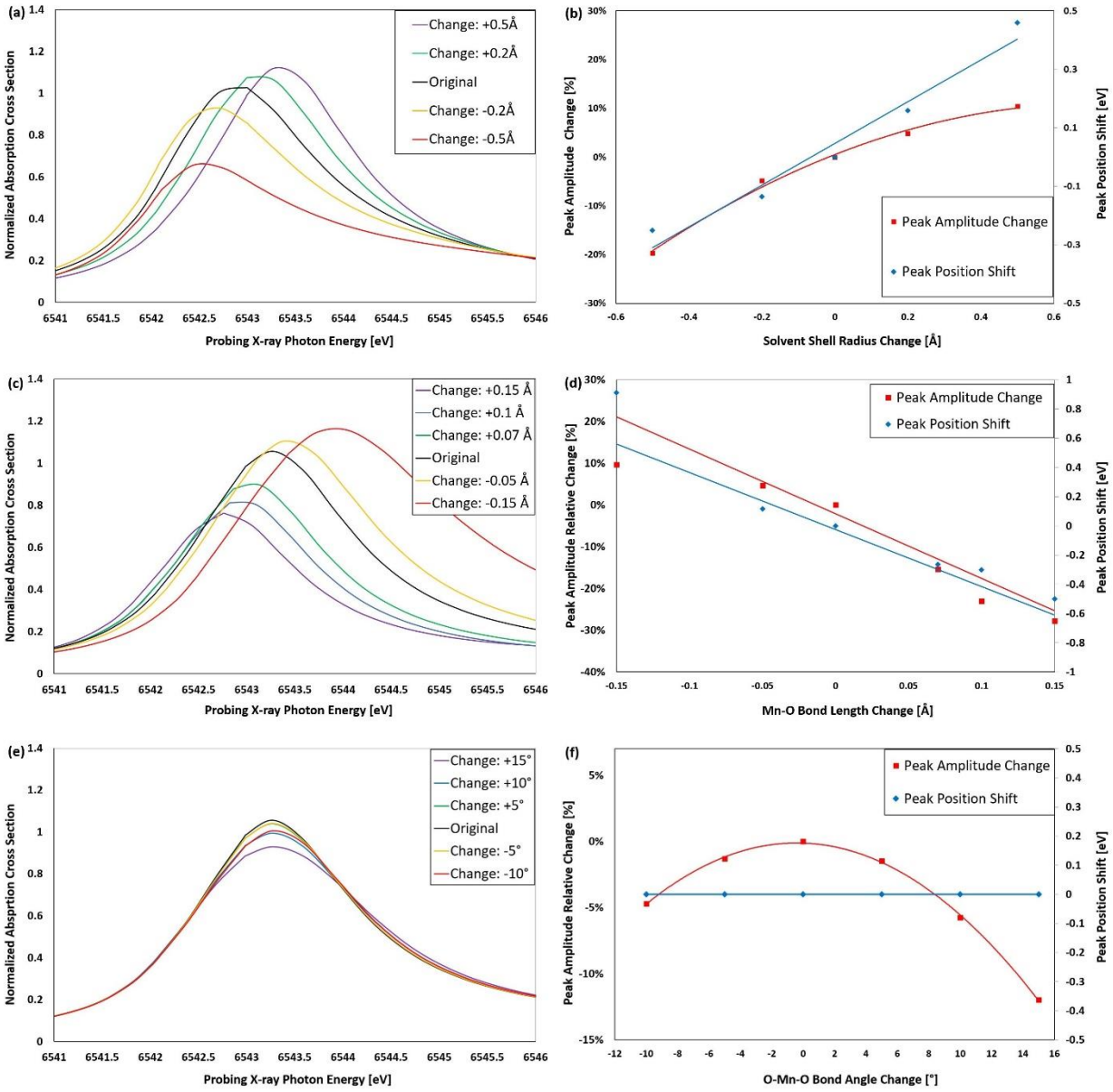

Figure 2 (**a**). The XAS of configurations with systematically varied solvent shell radius. (**b**). The relative absorption peak amplitude change and peak position shift shown in (a). (**c**). The XAS of solute configurations with varied Mn-O bond length. (**d**)**.** The relative absorption peak amplitude change and peak position shift shown in (c). (**e**). The XAS of solute molecules with varied O-Mn-O bond angle. (**f**). The relative absorption peak amplitude change and peak position shift shown in (**e**)

electrostriction inducing a transient grating. The fundamental phonon frequency is 13.5 GHz, which corresponds to the lower-frequency oscillation shown in FIG. 1. Using the refractive index *n = 1.33* and the transient grating wavelength $\lambda_{grating} = \lambda_{laser} / 2n$ relationship, the interference period can be calculated to be 100 nm. This spatial period, combined with the 13.5-GHz frequency, yield a sound speed of 1350 m/s, in agreement with the sound speed in liquid water, and a wave-vector of 0.062 nm^{-1}. The SH oscillation decays with a 38-ps time constant while the fundamental oscillation decays much slower with a time constant of at least 300 ps. Thus, the coupling between these two oscillations diminishes with time. This effect, as discussed below, is the result of the structural dynamics of water solvent.

In order to extract more information on the molecular level, calculations were conducted by systematically varying the molecular configurations of the solute-solvent-cluster/ solute-molecule understudy, calculating the spectra of the varied configurations and then comparing them with the spectra of the original ones. To determine the effect of the solvation shell radius on the XAS, we systematically varied the Mn-O bond lengths and solvation shell radius of the 10 snapshots from the QM/MM MD trajectories, calculated the XAS of these modified structures and plotted in FIG. 2a. For modeling the solvation shell change, each water molecule was radially translated away from/closer to the permanganate Mn atom. A quantitative evaluation of the solvent shell size changing effect was done by comparing the varied XAS peak position shift and peak amplitude relative change with respect to the original structure, as shown in FIG. 2b. To check the effect of single solute molecular structure change, the Mn-O bond lengths and O-Mn-O bond angles were varied and the results were presented from FIG. 2c to FIG. 2f.

It can be seen that Mn-O bond length and solvation shell radius changes modify both position and amplitude of the X-ray absorption line. Upon solvation shell expansion, however, the peak's amplitude change levels off, while its position still varies proportionally to the solvation shell radius. Importantly, the only motion that does not shift the spectra absorption peak position is the solute angular distortion with only the O-Mn-O bond angle changing.

The measured data were analyzed in more detail by simultaneously fitting a time and energy-dependent X-ray absorption profile to the X-ray spectra at $E_{measure}$ = *6542.0 eV, 6542.8 eV,* and *6543.5 eV*, see FIG. 3a-c. In order to allow for the SH waves to influence the X-ray absorption spectrum differently than the fundamental waves, this profile was written as the sum of two Gaussian curves, the first dependent on the time-zero-pulse and the fundamental oscillation and the second only dependent on the SH oscillation.

$$\Delta T_{E_{measure}}(t) = \underbrace{\frac{T_1}{\sqrt{2\pi}\,\sigma} e^{-\frac{1}{2}\left(\frac{E_{measure}-E_1}{\sigma}\right)^2}}_{\text{Pulse and fundamental oscillation}} + \underbrace{\frac{T_2}{\sqrt{2\pi}\,\sigma} e^{-\frac{1}{2}\left(\frac{E_{measure}-E_2}{\sigma}\right)^2}}_{\text{Second Harmonic oscillation}} \quad with \tag{3}$$

Parameter equations	*Fit – parameters*	*Number of Fit – par.*
$T_1 = T_{pulse}\ P(t) + T_{osc1}\ Osc_1(t)$	$T_{pulse}, t_{0,pulse}, \tau_{rise}, \tau_{fall}, T_{osc1}, t_{0,osc1}, \tau_{osc1}, \tau_{decay1}$	8
$E_1 = E_0 + E_{osc1}\ Osc_1(t) + E_{log}\ L(t)$	$E_{osc1}, E_{log}, t_{0,log}, \tau_{log}$	4
$T_2 = T_{osc2}\ Osc_2(t)$	$T_{osc2}, \tau_{osc2}, \tau_{decay2}$	3
$E_2 = E_0 + E_{osc2}\ Osc_2(t) + E_{log}\ L(t)$	E_{osc2}	1
$\sigma = const$	σ	1
$E_0 = 6542.8eV$		17
$L(t) = \frac{1}{1 + e^{\frac{t - t_{0,log}}{\tau_{log}}}}$		

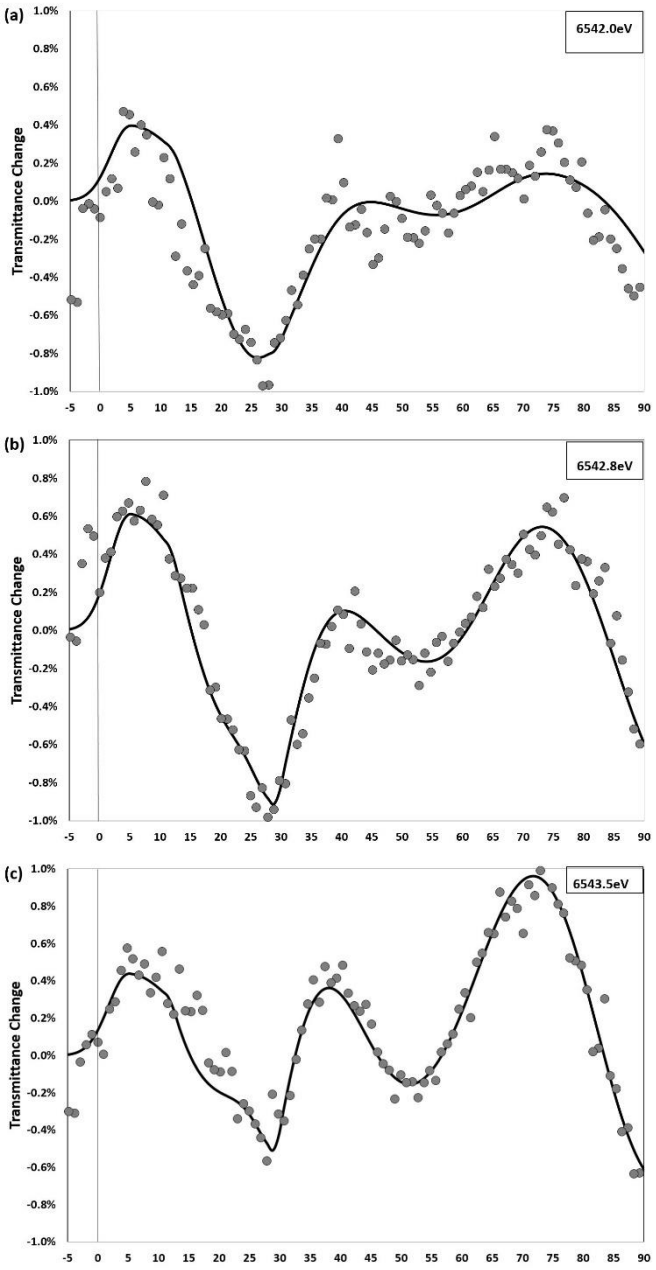

Figure 3 (a) (b) (c) Fitted X-ray transmittances measured at three different X-ray energies near the center (6542.8 eV) of the pre-edge line.

The Gaussian peaks were defined by their common center energy E_0, their common width σ, but separate amplitudes T_1, T_2 and separate energy positions E_1, E_2. The time-dependence of these Gaussian parameters were presented by combining amplitudes T_{pulse}, T_{osc1}, and T_{osc2}, describing the transmittance changes the same way as in equation (1), peak energy position shifts E_{osc1} and E_{osc2}, and time-dependent fit functions $P(t)$ and $Osc_i(t)$. Additionally, a logistics function $L(t)$ was used to describe the spectral shifts that may result from possible solvent shell reorganization and expansion caused by solute molecule electronic excitation, vibrational relaxation and a sudden system temperature jump after laser excitation.[34]
The resulting fits and time-dependent profiles of T_1, T_2, E_1, E_2, and E_{log} are shown in FIG. 4. and a full list of fit-parameters are listed in Table1. After the time-zero pulse the X-ray line amplitude oscillates at the 13.9 GHz fundamental frequency. Simultaneously, the line position exhibits an oscillatory deviation with 0.8-eV amplitude from the initial line position at 6542.8 eV. At 25ps, the lines shift by about 0.6 eV. The oscillation frequency is 3% higher than that shown in FIG.1.

This time coincides with the 1/e time of the pulse decay shown as grey curve in FIG. 1. We interpret the observed shift as a solvation shell radius increase. Our simulations show that simultaneous absorption peak amplitude and position changes are caused by solvation shell radius changes (FIG. 2a, 2b). They are accompanied by slight Mn-O bond length changes due to

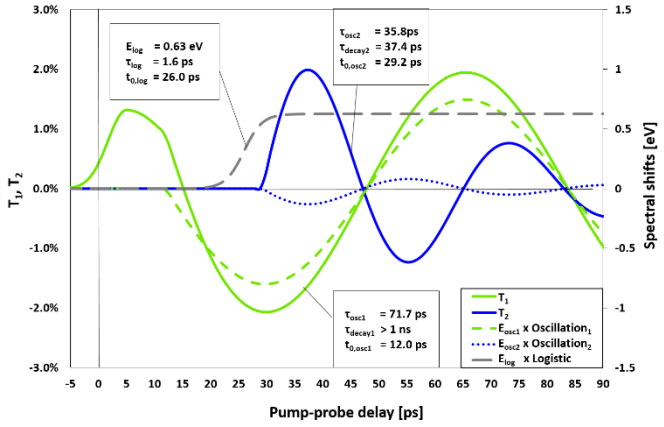

Figure 4 The time dependent profiles derived from fitting the spectra shown in Figure 3. The green solid line presents the 13.9-GHz oscillation signal due to the absorption peak amplitude change, the green dashed line represents the 13.9-GHz oscillation signal due to absorption peak position shift. The blue solid line presents the 27.9-GHz SH oscillation signal due to the absorption peak amplitude change, the blue dashed line represents the 27.9-GHz SH oscillation signal due to absorption peak position shift.

hydrogen bonds between the solute and solvent molecules (FIG. 2c, 2d). The solid and dashed curves with 13.9 GHz frequency in FIG. 4 oscillate simultaneously and in phase, indicating that these XAS oscillations are caused by solvation shell radius oscillations and the in phase oscillation of Mn-O bond length, a motion that corresponds to radial motion coherent oscillation. The 27.9-GHz curve in FIG. 4 is 90° phase shifted to the fundamental wave as expected for a 2nd harmonic wave. Its amplitude exhibits the same decay shown in FIG. 1. The oscillation frequency is 3% higher than that shown in FIG.1. Thus, while the oscillation frequencies shown in FIG.1 and FIG. 4 differ by about 3%, the higher-frequency oscillation frequency is always twice that of the fundamental oscillation. In neither fit was the ratio between these oscillations restricted in any way. Importantly, the peak position (blue dotted line) barely oscillates. Our previously presented simulations show that the only dynamics that changes the line amplitude without shifting the peak position is associated with permanganate angular distortion (FIG 2e, 2f) but not radial motions of the solvent of the Mn-O bond lengths. Since the complex is hydrogen-bonded to the surrounding water, angular distortion is coupled to transverse water motions which in turn suggest that the SH wave is a transverse acoustic wave. On the other hand, radial oscillation of the solvent shell of Mn-O bond lengths changes will be companied by local density fluctuations. So, the radial oscillation motion has the character of longitudinal waves. Granted the fact that in liquids collective modes cannot be strictly attributes to be pure longitudinal or transverse as in solids due to a large mixing symmetries[12], it is still reasonable to conclude that the two oscillations observed here are longitudinal-transverse couplings of phonons. An illustration of this longitudinal-transverse phonon coupling was presented in FIG. 5, with yellow curves representing the longitudinal phonon mode and green curves transverse ones. Yet, it is noted that these curves are just for illustrative purposes and are not from Molecular Dynamics simulations with these phonons existed in the system, thus do not carry any actual physical information. Combining the amplitude of the X-ray absorption peak position oscillation with our simulations, we estimate that the solvation shell radius oscillates with an amplitude of about 0.8 Å. Using the compressibility of water, we estimate that this diameter change corresponds to a pressure oscillation of about 1 GPa. Such high pressure will certainly cause the stress-strain tensor to be non-linear, which could be the reason for the 2nd harmonic generation in the first place.

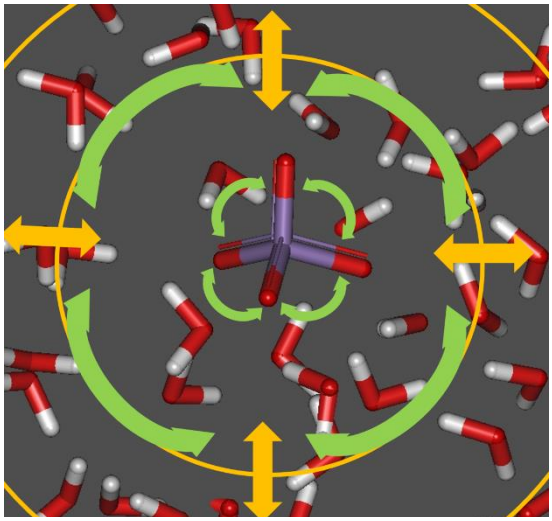

Figure 5 Illustration of the generated phonon coupling. The green curves represent the transverse mode and the yellow one longitudinal.

Pulse function parameters			
T_{pulse}	1.31%		
$t_{0,pulse}$	5.0 ps		
τ_{rise}	4.7 ps		
τ_{fall}	11.3 ps		
Oscillation functions parameters			
E_{osc1}	-0.83 eV	E_{osc2}	-0.16 eV
T_{osc1}	-2.15%	T_{osc2}	2.50%
τ_{osc1}	71.7 ps	τ_{osc2}	35.8 ps
$1 / \tau_{osc1}$	13.9 GHz	$1 / \tau_{osc2}$	27.9 GHz
$t_{0,osc1}$	12.0 ps	$t_{0,osc2}$	29.2 ps
τ_{decay1}	>1 ns	τ_{decay2}	37.4 ps
Logistics function parameters			
E_{log}	0.63 eV		
τ_{log}	1.6 ps		
$t_{0,log}$	26.0 ps		
Spectral line parameters			
E_0	6542.8 eV		
σ	0.86 eV	fwhm	2.02 eV

Table 1 Full list of the result fitting parameters listed in Equation (2) of the main text. Additionally, the full width at half maximum (fwhm) of the spectral lines calculated from σ is reported. The standard deviation of the fit is 0.015%.

Discussion

It should be noted that this is the first discovery of SH generation of local phonons in the vicinity of ions in aqueous solution, which provides new information about the structural properties of the HB network. The decay of the SH wave could be caused by an amplitude reduction of the 13.5-GHz pressure oscillation, or by a solvent density irreversible decrease around the solutes. This, however, would be visible in the simultaneous reduction of the measured fundamental amplitude and the shift of fitted *L(t)* function in the UXAFS data, which is not the case. We propose that the structural changes of the HB network in the domain around our solute diminish the coupling between fundamental and the SH wave, leading to the observed SH-decay. One such coupling mechanism could be the short-lived existence of glass-like stiffness around the probing solute molecules. Then, there should exist a region around the solute molecule with a structural relaxation time longer than the relaxation time in neat water. The measured 37-ps SH decay time can serve as a lower limit of the structural relaxation time of the solute domains in our system. Since the 37-ps relaxation time is longer than the inverse frequency of the 27.9-GHz phonons, the phonons are in the high-frequency limit of the HB network in the solute domain.

The glass-like character can also be inferred from the sound speed of the measured 27.9-GHz phonons. Combining the 27.9 GHz frequency and the 100nm wave-length, the SH phonon propagation speed can be calculated to be 2790 m/s. $c_{\infty, shear}$ is related to the shear modulus G of the bulk and the mass density ρ through

$$G = c_{\infty,shear}^2 \rho \cdot \quad (4)$$

The solution's density is about 1 kg/L at room temperature. Inserting this value and the measured c_∞ = 2790 m/s into eq. (1) we obtain a bulk modulus of 7.8 GPa. For reference, this modulus is larger than the (low-frequency) value of many plastics; the shear modulus of liquids below the high-frequency limit vanishes. Clearly, the high-frequency behavior of our solution is glass-like. The non-vanishing shear modulus is more characteristic of solids than liquids. The transverse phonon wave-number is 0.126 nm^{-1}. This is a clear deviation from the properties of neat water reported in the literature. Molecular Dynamics simulations of neat water reveal that the transverse mode cannot propagate and is relaxational-like with wave-vectors lower than 2 nm^{-1}.[12] Thus, in neat water the 27.9-GHz oscillation would not occur. The difference between neat water and solutions can be explained by the fact that the structural relaxation time of the solute domains under study is longer than the subpicosecond time scale in neat water. Specifically, the inverse angular frequency τ of the 27.9-GHz phonons are 5.6 ps, much higher than the ~0.6 ps structural relaxation time of HB network in neat water.

Our measured high-frequency sound speed is in good agreement with the speed measured by Brillouin Light Scattering in neat water at 300K.[10] However, in neat water a tens-of-GHz soundwave propagates with the adiabatic sound speed (approx. 1.5 km/s) while the high-frequency sound speed is a parameter obtained from the viscoelastic model. In our electrolytic solutions, in contrast, we directly measure that the 27.9-GHz phonons propagate with the high-frequency sound speed. We note that the Brillouin scatter measurements detect longitudinal phonons, while our data indicates that the 27.9-GHz phonons have substantial transverse character. It is not obvious at this time why both high-frequency speeds are nearly identical. This may be a coincidence or an indication that our observed transverse mode has significant longitudinal character at some distance from the X-ray-probed solute molecules. Our results provide additional information about the effects that solutes exert on the HB network in aqueous solutions. Previously, such data were obtained from techniques such as SAXS, hyper-Rayleigh and second harmonic light scatteing.[6, 7, 35] Our results indicate that the existence of charged solutes will increase the structural relaxation time of the HB network around them by possibly decreasing the mobility of water molecules in the solvent shells.

The observed longitudinal-transverse phonon coupling bears strong resemblance to the rotation-longitudinal acoustic phonon coupling proposed by D. Shelton, which is believed to be the reason of the HRS detected transverse polar collective modes in liquid water.[9] The discovery of the phonon coupling

in this article supports the proposed long-range phonon mode coupling effect for the explanation of the long-range dipole moment correlation. The oscillatory features shown in FIG. 1 and FIG. 4 clearly imply the existence of coherent oscillation of groups of molecules. Neither the spatial extent of the coherent oscillations nor the propagation length of the phonons can be exactly determined in our experiments due to the fast decay of the transverse phonon and the fact that our XAS probe can only probe the dynamics around the solutes. Yet, some qualitative estimates can be made about the phonon propagation length. Combining the 38-ps decay time and the sound speed of 2790 m/s, the SH phonon propagation length is estimated to be 106 nm. This value is thus the estimate for the lower limit of the spatial extent over which the transverse mode coherent oscillations exist. It is in qualitative agreement with the "solute domains" measured with Static Light Scattering (SLS) and Dynamic Light Scattering (DLS) techniques.[36] It has been decades that DLS and SLS measurements show the inhomogeneities in aqueous solutions, generally on the scale of several hundred nanometers. These inhomogeneities were identified as high solute concentrations domains.[37] It was confirmed by Sedlák *et al.* that these domains exist in more than one hundred solute-solvent combinations.[37-39] These domains can be descripted as "loose aggregates", with solute concentrations and domain densities higher than the rest of the bulk solution and are of nearly spherical shape.[37, 39] They additionally concluded that the formation of these domains relies on the directed HBs between solute and water molecules that are hydrogen-bonded themselves.[38] Given the fact that there do exist HBs between the MnO_4^- solute molecules and water solvent shells, these solute domains are highly likely to be formed in our sample solution and the signal we observed may actually be from phonons propagating inside of these solute domains. If this is true, our results could serve as a characterization of the colligative properties inside of solute domains.

Conclusions

We measured the generation of SH phonons in aqueous solution using picosecond time resolved X-ray absorption spectroscopy, with both longitudinal and transverse phonons unambiguously identified. The results presented here are the first discovery of low wave-number transverse mode propagation in aqueous solutions and the first experimental discovery of the longitudinal-transverse phonon coupling in solutions. The slow decay of the SH conversion efficiency implies the presence of glass-like, high-frequency stiffness around the solutes. The decay time of the SH conversion efficiency can serve as a new method to measure the lower limit of structural relaxation time of the hydrogen bond network around charged solute molecules. The relaxation time is found to be one magnitude higher than that of HB network in neat water. The effect of solutes is the reduction of the high-frequency limit, i.e. they enable high-speed phonon propagation at much lower frequencies than possible in neat water.

Acknowledgements

C.R.P. and Y.J. acknowledge support from the U.S. Department of Energy under grant DE-FG02-08ER15937. The work at the Advanced Photon Source was supported by the U.S. Department of Energy, Office of Basic Energy Sciences under Contract DE-AC02-06CH11357. We thank R. M. Stratt for helpful discussions and H. Wen and Y. Li for providing laser technical support.

Notes and references

1. N. Agmon, *J. Phys. Chem.*, 1997, **100**, 1072-1080.
2. D. C. Elton and M. Fernandez-Serra, *Nat. Commun.*, 2015, **7**, 10193.
3. A. Beneduci, *J. Mol. Liq.*, 2008, **138**, 55-60.
4. F. Sette, G. Ruocco, M. Krisch, C. Masciovecchio, R. Verbeni and U. Bergmann, *Phys. Rev. Lett.*, 1996, **77**, 83-86.
5. A. W. Omta, M. F. Kropman, S. Woutersen and H. J. Bakker, *Science*, 2003, **301**, 347-349.
6. Y. Chen, H. I. Okur, N. Gomopoulos, C. Macias-Romero, P. S. Cremer, P. B. Petersen, G. Tocci, D. M. Wilkins, C. Liang, M. Ceriotti and S. Roke, *Science Advances*, 2016, **2**, e1501891.
7. C. Chen, C. Huang, I. Waluyo, T. Weiss, L. G. M. Petterssond and A. Nilsson, *PCCP*, 2015, **17**, 8427-8430.
8. Y. Marcus, *Chem. Rev.*, 2009, **109**, 1346-1370.
9. D. P. Shelton, *J. Chem. Phys.*, 2014, **141**, 224506.
10. S. C. Santucci, D. Fioretto, L. Comez, A. Gessini and C. Masciovecchio, *Phys. Rev. Lett.*, 2006, **97**, 225701.
11. A. Cunsolo, G. Ruocco, F. Sette, C. Masciovecchio, A. Mermet, G. Monaco, M. Sampoli and R. Verbeni, *Phys. Rev. Lett.*, 1999, **82**, 775-778.
12. M. Sampoli, G. Ruocco and F. Sette, *Phys. Rev. Lett.*, 1997, **79**, 1678-1681.
13. B. W. Adams, C. Rose-Petruck and Y. Jiao, *J. Synchrotron Rad.*, 2015, **22**, 1022-1029.
14. M. Chollet, B. Ahr, D. A. Walko, C. Rose-Petruck and B. Adams, *IEEE J. Sel. Topics Quantum Electron.*, 2011, **18**, 66 - 73.
15. B. Ahr, M. Chollet, B. Adams, E. M. Lunny, C. M. Laperlec and C. Rose-Petruck, *PCCP*, 2011, **13**, 5590-5599.
16. J. Enkovaara, C. Rostgaard, J. J. Mortensen, J. Chen, M. Dulak, L. Ferrighi, J. Gavnholt, C. Glinsvad, V. Haikola, H. A. Hansen, H. H. Kristoffersen, M. Kuisma, A. H. Larsen, L. Lehtovaara, M. Ljungberg, O. Lopez-Acevedo, P. G. Moses, J. Ojanen, T. Olsen, V. Petzold, N. A. Romero, J. Stausholm-Moller, M. Strange, G. A. Tritsaris, M. Vanin, M. Walter, B. Hammer, H. Hkkinen, G. K. H. Madsen, R. M. Nieminen, J. K. Norskov, M. Puska, T. T. Rantala, J. Schiotz, K. S. Thygesen and K. W. Jacobsen, *J. Phys.: Condens. Matter*, 2010, **22**, 253202.
17. L. H. J. Mortensen, and K. W. Jacobsen, *Phys. Rev. B*, 2005, **71**, 35109.
18. A. H. Larsen, M. Vanin, J. J. Mortensen, K. S. Thygesen and K. W. Jacobsen, *Phys. Rev. B*, 2009, **80**, 195112.
19. J. P. Perdew, K. Burke and M. Ernzerhof, *Phys. Rev. Lett.*, 1996, **77**, 3865-3868.

20. S. R. Bahn and K. W. Jacobsen, *Computing in Science & Engineering*, 2002, **4**, 56-66.
21. E. Ö. Jónsson, K. W. Jacobsen, K. S. Thygesen and J. Ulstrup, PhD Thesis, Technical University of Denmark, 2014.
22. A. O. Dohn, E. O. Jonsson, K. S. Kjær, T. B. v. Driel, M. M. Nielsen, K. W. Jacobsen, N. E. Henriksen and K. B. Møller, *J. Phys. Chem. Lett.*, 2014, **5**, 2414-2418.
23. A. O. Dohn, *Transient Changes in Molecular Geometries and How to Model Them*, Springer International Publishing, 2014.
24. A. Rappe, C. Casewit, K. Colwell, W. G. III and W. Ski, *J. Am. Chem. Soc.*, 1992, **114**, 10024-10035.
25. J. J. Rehr, J. J. Kas, F. D. Vila, M. P. Prange and K. Jorissen, *PCCP*, 2010, **12**, 5503-5513.
26. J. J. Rehr, J. J. Kas, M. P. Prange, A. P. Sorini, Y. Takimoto and F. D. Vila, *Comptes Rendus Physique*, 2009, **10**, 548-559.
27. J. J. Rehr and R. C. Albers, *Rev. Mod. Phys.*, 2000, **72**, 621-654.
28. J. J. Rehr and A. L. Ankudinov, *J. Synchrotron Rad.*, 2001, **8**, 61-65.
29. F. D. Groot, G. Vanko and P. Glatzel, *JOURNAL OF PHYSICS: CONDENSED MATTER*, 2009, **21**.
30. J. W. Smith, R. K. Lam, O. Shih, A. M. Rizzuto, D. Prendergast and R. J. Saykally, *J. Chem. Phys.*, 2015, **143**, 084503.
31. S. De Silvestri, J. G. Fujimoto, E. P. Ippen, E. B. Gamble, Jr., L. R. Williams and K. A. Nelson, *Chem. Phys. Lett.*, 1985, **116**, 146-152.
32. R. W. Boyd, *Nonlinear Optics*, Academic Press, Boston, 1992.
33. B. J. Berne and R. Pecora, *Dynamics Light Scattering: With Applications to Chemistry, Biology and Physics*, Dover Publications, Mineola, 2000.
34. C. R. M. Donald G. Lee, Takatoshi Hayashi, John I. Braurnan, *J. Am. Chem. Soc.*, 1987, **109**, 3003-3010.
35. D. P. Shelton, *J. Chem. Phys.*, 2009, **130**, 114501.
36. Y. Georgalis, A. M. Kierzek and W. Saenger, *J. Phys. Chem. B*, 2000, **104**, 3405-3406.
37. M. Sedlak, *J. Phys. Chem. B*, 2006, **110**, 4329-4338.
38. M. Sedlak, *J. Phys. Chem. B*, 2006, **110**, 13976-13984.
39. M. Sedlak, *J. Phys. Chem. B*, 2006, **110**, 4339-4345.